DYMAT 2009 (2009) 575–581

DOI: 10.1051/dymat/2009082

Fracture behavior of a Zr-metallic glass under dynamic compression

Z. Ling, J.X. Meng, M.Q. Jiang and L.H. Dai

State Key Laboratory of Nonlinear Mechanics, Institute of Mechanics, Chinese Academy of Sciences, 100190 Beijing, PR China

Abstract. Dynamic planar compressive experiments on a typical tough Zr-BMG (Bulk Metallic Glass) were carried out under impact velocity of 500–600 m/sec and strain rate of 10^6/s. The fracture surface of samples exhibits different fracture patterns at different parts of the sample. At a corner close to the front loading boundary, fracture patterns from the free edge toward the centre changed from equiaxial veins in microscale to periodic corrugations in nanoscale; in the middle of the sample, the fracture surface contains glazed zones laid out orderly along the same boundary. FEM simulation was performed to investigate the stress distributions in the impacted sample under a short duration impact loading. It has revealed that the fracture patterns changing from the free edge toward the centre were resulted from the fracture modes' changing from the tensile dominant fracture to the shear dominant fracture. Whereas at the middle part of the sample, fracture initiated from several parallel shear bands propagating close to the same boundary is due to a large strain or much higher shear stress in this area.

1. INTRODUCTION

Bulk metallic glasses (BMGs) and their fracture behavior have received wide attention because of their excellent mechanical properties and functional applications, resulting directly from their unique amorphous structures. As a lack of long-range order in the atomic structures, micro-mechanisms of inelastic deformation of BMGs [1–3] are no longer related to dislocation-based mechanisms that always characterize the plastic deformation of crystalline metals. Thus BMGs have no strain hardening and their inelastic deformation is characterized only by shear and normal stresses; fracture typically occurs after a very small inelastic strain in tensile or substantial inelastic strain level under quasi-static compression [1–6].

Being quite different from those of crystalline solids, BMGs' fracture and failure behavior under normal stresses have currently been investigated in the quasi-static regimes [1–3, 5–6] with a considerable interest. However, few studies for deformations and fracture behavior of BMGs in the high strain rate regime have been reported. Recently dynamic compressive behavior of BMGs was explored using the split hokinson bar technique at strain rates up to $10^3\,s^{-1}$ [7–8]. Whereas hardly has any research of the BMGs' fracture behavior under much higher train rate loading, strain rate up to $10^{5\text{-}6}\,s^{-1}$, been reported [9–11].

In this paper, we reported on the dynamic compressive fracture behavior of a Zr-BMG under planner compressive impact. A light gas gun had been adopted to carry out the dynamic experiments. Close-up descriptions of the fracture surface of the sample fragments and FEM simulations to the dynamic compressive samples were performed to further understand the tough BMGs' dynamic fracture behavior under much high strain rate loading.

2. EXPERIMENTAL PROCEDURE

2.1 Materials and experiments

The material used in this experiment was $Zr_{41.2}Ti_{13.8}Cu_{12.5}Ni_{10}Be_{22.5}$ [Vit.1] rods ($\Phi 8 \times 30$), with Young's modulus E = 96 GPa, Poisson's ratio v = 0.36, and tensile strength, $\sigma_{tensile} = 1.9$ GPa. BMG samples were identified to be full amorphous state by conventional x-ray diffraction before high-speed impact experiments. The samples were machined to disks of 8 mm in diameter and 0.3 mm in thickness for planner impact tests.

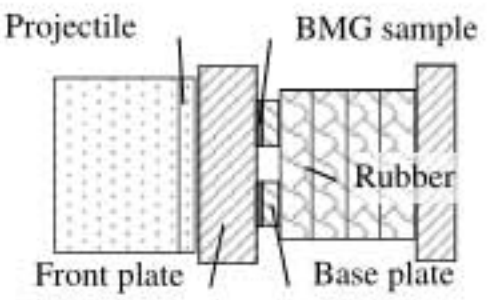

Figure 1. Scheme of a planner compressive loading set.

Impact tests were performed with a 101 mm single-stage light gas gun at LNM Laboratory, details of configuration of the light gas gun can be found in earlier reports elsewhere [12]. Figure 1 presents a scheme of a loading set, by which samples under planner compressive impact can be conducted. As shown in the figure, a BMG sample is sandwiched between a front and a base steel plate; the thicknesses of the front and base plates are 30 mm and 1 mm, respectively. Both front and base plates are of higher wave impedance compared with the BMG sample. Table 1 displays principal mechanical properties of BMG samples, projectiles, the front and base plates in the impact experiments. Additionally, the rotation of the projectile launched in the gun tube was less than 1–2°, which guarantees the success of simultaneous impact to several samples in one shot.

Figure 2 is the Z-t profile of stress wave propagation in the sample during impacting, where Z-axial denotes the loading direction along the thickness of the sample and the time-axial is the propagating time of stress wave. The launched flyer plate at the speed of 500–600 m/s impacted onto the front steel plate. At the moment of impact, planar compressive shock wave generated in the front plate propagates to the BMG sample and then compressive waves reflected from the interface between the BMG sample and the base plate. Taking into account of thickness and material properties of the sample, front and base plates, the normal stress the BMG sample is subjected to is compressive during impact. As shown in the figure, I-VI denote stress durations with different stress amplitudes in the sample. Here the normal stress, caused by sparse-waves reflected from another interface between the base plate and rubber behind, is neglected.

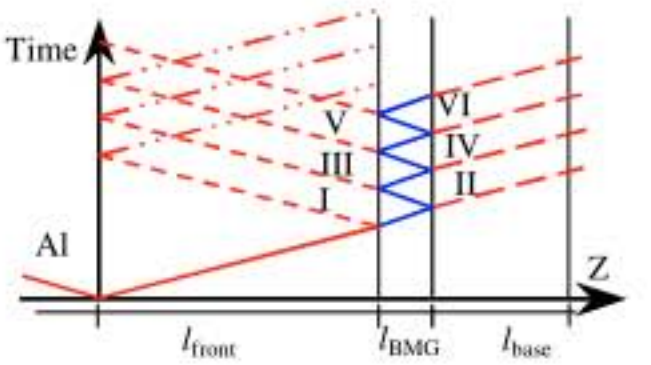

Figure 2. Stress wave propagating in the BMG sample, front and base plates; where l_{front}, l_{base} and l_{BMG} are thickness of the front, base plates and BMG sample, respectively.

Dynamic compressive tests were performed at impact velocities of 563.8–600 m/s. Table 2 lists the axial compressive stresses, σ–I to σ–VI, BMG samples subjected in durations from I to VI at

Table 1. Principal physical parameters of materials and thickness of plates in current impact experiments.

	Materials	Density (g/cm^3)	Modulus (GPa)	v	$\sigma_{tensile}$(GPa)	Thickness (mm)
Projectile	Al	2.7	72	0.33	-	10
Front plate	Steel	7.8	210	0.29	-	3.0
Sample	Zr-BMG	6.0	96	0.36	1.9	0.3
Base plate	Steel	7.8	210	0.29	-	1.0

Table 2. Axial compressive stress of the sample in the loading direction at different loading durations.

Impact Velocity (m/sec)	Materials	σ–I (GPa)	σ–II (GPa)	σ–III (GPa)	σ–IV (GPa)	σ–V (GPa)	σ–VI (GPa)
563.8	Zr-BMG	4.35	5.47	5.75	5.82	5.91	6.03
600	Zr-BMG	4.63	5.82	6.12	6.19	6.29	6.41

impact velocities of 563.8 and 600 m/s. As shown in the table, under impact velocity of 600 m/s, compressive stress to which BMG samples subjected is initially 4.63 GPa and gradually becomes higher with the duration increased.

Close-up observations with a high resolution scanning electronic microscopy (HRSEM) (FEI-Sirion NC HRSEM with 1.5 nm resolution) were performed to the recovered, impacted BMG samples.

2.2 Experimental results

Figure 3 presents micrographs of a fragment piece of the sample for the impact velocity of 563.8 m/s. The fragment has two fracture surfaces with wavy edges in the radial direction of the disk-shaped sample and, both surfaces are almost perpendicular to each other, resulting in the fracture in the radial direction of the sample. At a corner of the fragment, marked by A, the fracture edge has an angle less than 45° to the tangent of the sample edge. Obviously, such a fracture edge illustrated that fracture occurred in the loading plane normal to the axial compressive loading and therefore was caused by stresses in the same plane. Thus this fracture at the corner was resulted in stresses tangent to the sample edge, which is consistent with the fracture features of BMGs under normal stress [4]. Figure 3b is an overlook of a fracture surface corresponding to the zones from A to B marked in Figure 3a. The fracture surface is so rugged that several arc zones were formed to be orderly arrayed. Figures 3c and 3d show enlarged images of two arc zones as rectangles marked in Figure 3b. Each arc zone is an incline consisting of a glazed core and a rough part, sloping up from left to right in the figures. The slope orientation from the glaze to the rough part is indicated along the arrows and has an angle to the compressive loading direction (Figures 3c and 3d). As these zones were small surfaces along which failure occurred, it is clear that the failure oriented at an angle to that compressive loading direction.

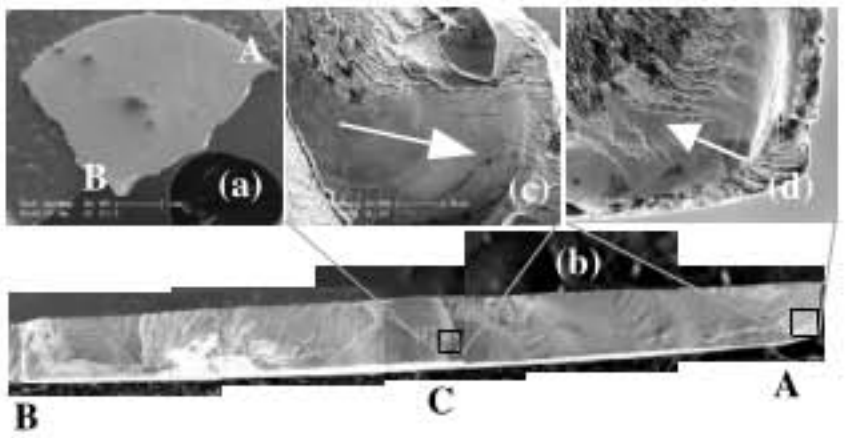

Figure 3. Photographs of a typical fragment of the sample under impact velocity of 563.8 m/s, (a) A fragment fractured from the sample, where letter "A" denotes the free edge and "B" the center of the sample; (b) An overlook of a fracture surface from A to B of the fragment, where zones in squares are local at middle and free edge of the sample, respectively; (c) Detail of small glaze zone marked with a rectangle above C in (b); (d) One corner at the free edge, marked with A in (b).

Compressive failure along a plane, about 42°–46° to the loading direction [4, 11], has been commonly observed in BMGs' mechanical testing. This is recognized to be caused by shear band propagation. Thus it clearly suggested that several arc zones or small failure surfaces in a fragment would be instantly induced by several shear bands' propagating. Under impact velocity of 563.8 m/s, the sample is subjected to such large strain that several shear bands at

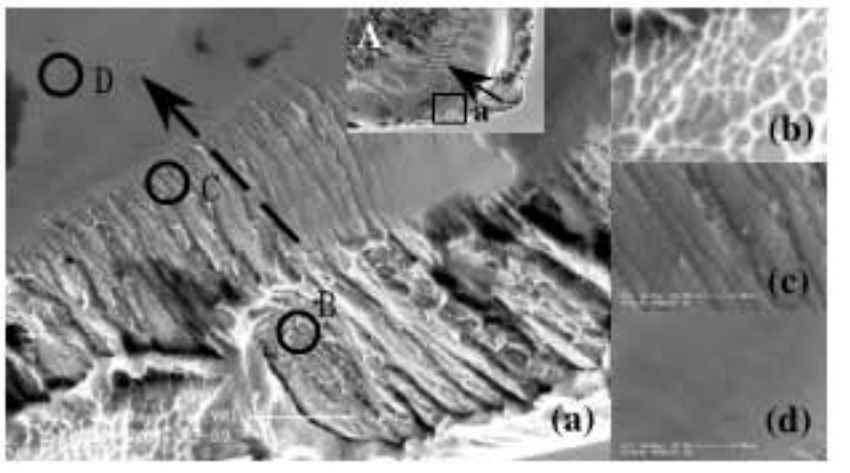

Figure 4. Detail fractograph of zone-a as inserting figure. (a) micromorphologies evolution in zone-a, along arrow's direction: from B to D: (b) Vein patterns; (c) Dimples structures and (d) Periodic corrugations.

different planes, with angles to the axial compressive loading, had to begin propagating simultaneously. In this case, there were several small failure surfaces at different planes formed. Particularly under impact loading, several parallel shear bands would form and start to propagate in a large strain zone. Thus several small failure surfaces would form along those paralleled shear bands in such a large strain zone. That is why several arc zones arrayed orderly are built up as shown in Figure 3b. In addition to this, the arc zones of the glazed and rough parts are also in accordance with those features of fracture surface, known as "mirror, mist, and hackle" as well as more special micro-patterns, which are usually observed on fracture surface of BMGs under mechanical testing [4–6, 11]. As illustrated in Figures 3c and 3d, arrows indicated from the glazed to rough parts in small fracture surfaces, represent the directions in which fracture or shear bands are propagating. Moreover the glazed zones are almost close to the sample edges, no matter whether they are in the middle (Figure 3c) or at a corner (Figure 3d). This indicates that, in this sample, fracture or shear bands' propagation originates from the boundary B-A.

Figure 4 displays the micrographs of the zone at the corner-A indicated in Figure 3b. Figure 4a is an enlarged fractography in the zone that is square-shaped in the small photo on the top and corresponds to the a-zone. In the figure, fractography transition from a vein pattern to a dimple structure, then to a periodic corrugation pattern is exhibited. Three zones from B to D as illustrated with arrows in Figure 4a and their details are clearly shown in Figures 4b–4d. It is noted that in Figure 4b, veins in zone-B are approximately of equiaxially shaped, which means that zone-B is tensile stress dominating. Orderly zone-C is of a dimple structure zone (Figure 4c) and zone-D is at the glazed or mirror zone and presents a periodic corrugation pattern in its enlarged image (Figure 4d). Such fractographic transition along the fracture propagation direction has been analyzed and its different fractographic patterns in nanoscales have also been recognized as evidence for the dynamic fracture instability along the fracture propagation direction of Zr-BMGs [13].

It is clear that fractographic patters are final tracks of interacting of BMGs' intrinsic characters and BMG's micro-mechanical state. Whereas, some essential points need further understanding to the present samples, such as why fracture or shear bands' propagation originates from boundary B-A or from one corner close to A, what stresses dominate or urge such fracture propagating and when fracture occurs at such short loading duration so on. To answer above questions, it is necessary to solve stress distributions in samples under dynamic planner compressive loading by FEM simulations.

3. SIMULATION MODELS AND RESULTS

3.1 Simulation models

Axisymmetric simulations of the impact compressive sample were performed using ABAQUS. To follow the real loading environment of the dynamic loading, an FEM model was built with two loading boundaries, from which a sample was initially compressed by the front plate and then by the base plate as illustrated in Figures 1 and 2. Especially, the disk-shaped sample's free edge was taken into account in the FEM model.

Figure 5 is a schematic of the simulation model. An axisymmetric half-section of a sample is adopted and B-A is the front loading boundary and B'-A' the back one, where A-A' is the free edge of the sample (Figure 5a); l_{BMG} is the sample thickness, 330 μm, and

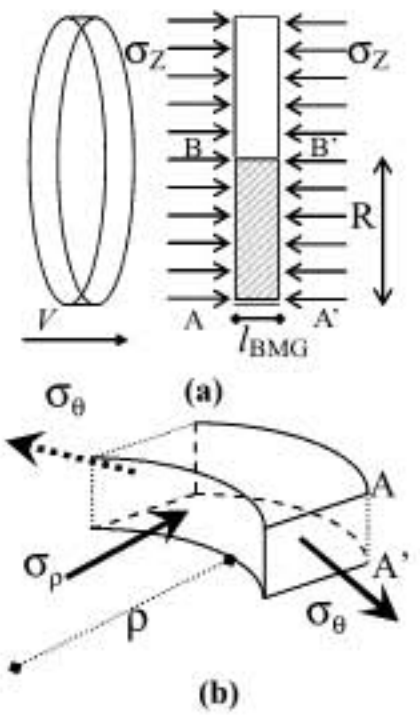

Figure 5. Scheme of FEM model. (a) Axisymmetric half-section of a disk-shaped sample (BAA'B'); (b) A zone close to the free edge AA' and σ_θ and σ_ρ are tangent and radial stress.

R is the radius of the sample, 4000 μm. Figure 5b sketches the zone close to the free edge of A-A', where compressive loading is along A-A' (thickness), the radial and tangent directions of the sample are denoted by ρ and θ, respectively. It is noted in the figure that tangent stress σ_θ is tensile while radial stress σ_ρ is compressive along the free edge. To get accurate results, the FEM model's elements in the zone close to the free edge were meshed at a finer scale than the other parts of the sample. In addition, Zr-BMG's elastic material parameters, shown in Table 2, were used in present simulations, focusing on stress distributions in the sample under dynamic compressive loading.

3.2 Simulation results

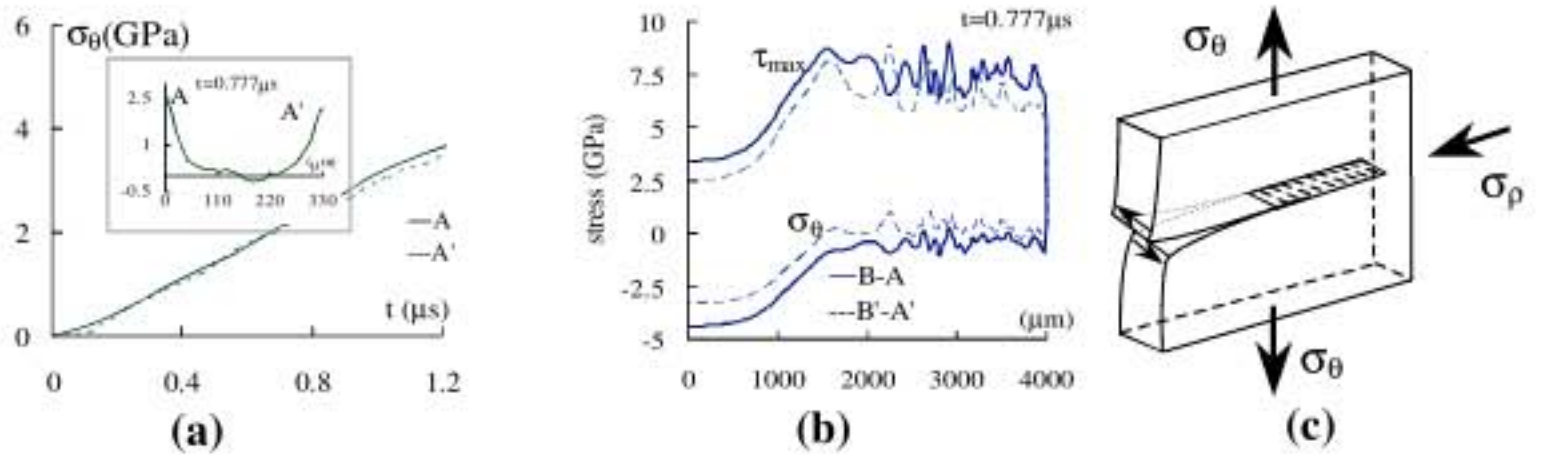

Figure 6. Stress distributions in the BMG sample at V = 600 m/s. (a) σ_θ at A and A' in the sample' during impact compressive loading (insert showing its distributing along A-A' at t = 0.777μs); (b) τ_{max} and $\sigma_{,\theta}$ along B-A and B'-A' at t = 0.777μs. (c) Fracture occurred in the zone close to a free edge of the sample.

Simulation stress distributions in the impacted sample under velocity of 600 m/sec are displayed in Figure 6. Figure 6a shows tangent stress σ_θ at two corners, A and A', at a time of 1.35 μs after the impact loading started to apply. The magnitudes of σ_θ at two corners increase linearly with the time duration. Since Zr-BMG's tensile strength is 1.9 GPa (Table 1), the sample would be fractured at the free edge once σ_θ reaches at or over BMG's tensile strength. According to the curves of σ_θ-time, at t = 0.777 μs, the magnitude of σ_θ at two corners are over 1.9 GPa. The inserted figure in Figure 6a exhibits the σ_θ distribution along the sample thickness, from corner-A to corner-A' at t = 0.777 μs. At this moment the magnitudes of σ_θ are 2.5 and 2.2 GPa at corner-A and corner-A', respectively.

Figure 6b shows distributions of the maximum shear stress τ_{max} and σ_θ along two loading boundaries, B-A and B'-A', at t = 0.777 μs. Except for two corners, σ_θ along two boundaries are not greater than the tensile strength of the Zr-BMG. Particularly, along the radial, σ_θ is always compressive from 0 to 2000 μm and varies up-and-down around zero from 2000 μm to the free edge. Simultaneously, the magnitude of τ_{max} varies between 2.5–8.5 GPa along B-A and B'-A' and, down to 3.4 GPa at corner-A and 2.6 GPa at corner-A'. Especially, higher τ_{max}, 7.5–8.5 GPa, appears in the middle of the sample, 1500–3000 μm away from the centre. Moreover, from 2500 μm toward the free edge, several steeps with both ups and downs appeared in both σ_θ and τ_{max} curves, are attributed to disturbances of stress waves from corners and boundaries of the sample. Accordingly, Figures 6a and 6b distinctly have revealed that, at t < 0.777 μs, fracture occurs firstly at corner-A and is initially induced by tensile stress σ_θ due to the BMG's low tensile strength. However once the tensile failure has initiated at the corner, localized shear deformation occurs in the zone adjacent to the crack. In this case, the fracture or failure propagation is dominated by the high shear stress or shear strain.